Supporting Information

A spontaneously healable robust ABA tri-block polyacrylate elastomer with multiphase structure

Wenyan Wang, Zijian Guo, Zongxu Liu, Shuai Qiu, Chunmei Li * and Qiuyu Zhang *

School of Chemistry and Chemical Engineering, MOE Key Laboratory of Material Physics and Chemistry Under Extraordinary Conditions, Key Laboratory of Special Functional and Smart Polymer Materials of Ministry of Industry and Information Technology, Northwestern Polytechnical University, Xi'an, Shaanxi, 710072, P. R. China.

**Corresponding authors: Chunmei Li; Email: lichunmei@nwpu.edu.cn and Qiuyu Zhang; E-mail: qyzhang@nwpu.edu.cn; qyzhang1803@gmail.com*

Synthesis of S, S'-bis (α, α'-dimethyl-α"-propargyl acetate) trithiocarbonate

The RAFT agent S, S'-bis (α, α'-dimethyl-α"-acetic acid) trithiocarbonate (BDATC) was synthesized by following the previously published works[1-5]. Typically, the procedure was as follows. A 250 mL round bottom flask with carbon disulfide (3.4250 g), acetone (6.5380 g), chloroform (13.4375 g), tetrabutylammonium bromide (0.2858 g) and mineral oil (15 mL) was cooled to 0 °C under vigorous stirring. Subsequently, under an atmosphere of highly pure argon, 25.2000 g 50 wt% aqueous solution of NaOH was slowly added within 50 min. The reaction was heated to 25 °C and left stirring for 12 h. After the reaction was complete, 100 mL deionized water was added to dissolve the resulting solids, followed by 15 mL HCl was added to acidize the aqueous phase and the reaction mixture was stirred intensely for another 50 min. Insoluble solid was filtered out and washed with deionized water for 3 times. A bright yellow product was obtained with the yield of 63% after recrystallization in the mixture of toluene and acetone.

Measurements

Fourier transform infrared spectroscopy (FTIR): Infrared transmission spectra were recorded using a BRUCKER TENSOR27 spectrometer. The number of scans was 16 and the wavenumber scale was from 4000 cm^{-1} to 400 cm^{-1}.

Gel permeation chromatography (GPC) was performed on a Waters1515 system equipped with an OPTILAB rEX detector running on THF at 40 °C with a flow rate of 1 $mL \cdot min^{-1}$. Polystyrene samples of narrow molecular weight distribution were employed as standards.

Nuclear Magnetic Resonance (NMR): ^{1}H-NMR and ^{13}C-NMR were characterized on a Bruker Avance 400 MHz spectrometer. $CDCl_3$ and DMSO-d_6 were used as the solvents.

Thermogravimetric analysis (TGA) measurements were performed on TA Instruments Q500 equipment from 35 ^{o}C to 700 ^{o}C at a heating rate of 10 $^{o}C \cdot min^{-1}$ and kept at 100 ^{o}C for 10 min subsequently. And then cooled from 100 ^{o}C to 35 ^{o}C at a cooling rate of 10 $^{o}C \cdot min^{-1}$. Afterwards, the heat flow was recorded from 35 ^{o}C to 700 ^{o}C at a heating rate of 10 $^{o}C \cdot min^{-1}$ under nitrogen atmosphere.

Differential scanning calorimeter (DSC): Heat flow curves were obtained on Mettler Toledo. The sample was firstly heated from 25 ^{o}C to 130 ^{o}C and then cooled from 130 ^{o}C to -70 ^{o}C at a cooling rate of 10 $^{o}C \cdot min^{-1}$ to eliminate the thermal history. Afterwards, the heat flow was recorded from -70 ^{o}C to 130 ^{o}C at a heating rate of 10 $^{o}C \cdot min^{-1}$ under nitrogen atmosphere.

Atomic force microscopy (AFM) was performed in tapping mode using Bruker Dimension Icon. The films for AFM characterization were prepared by spin-coating from THF solvent onto silicon wafers at 1800 rpm for 12 s and then 2500 rpm for 20 s using a KW-4A spin-coater, and then were annealed in THF saturated vapor at 36 ^{o}C for 60 h.

Transmission electron microscope (TEM) was recorded on FEI Talos F200X TEM Schottky thermal field emission high resolution transmission electron microscope. The sample was dissolved in tetrahydrofuran to produce a solution with a mass fraction of 5%, which was added to the ultra-thin copper mesh. The solvent was volatilized and then observed by TEM. Optical test: UV-Vis transmission spectrum was measured by using UV-2550 (Shimadzu) spectrophotometer with the detection wavelength ranging from 800 nm to 200 nm.

Tensile experiments were performed on a SANS CMT 8505 tensile tester (equipped with 100N sensor). Uniaxial tensile measurements were carried out in air at room temperature with a loading rate of 50 $mm \cdot min^{-1}$. The dumbbell shaped samples were cut using a normalized cutter. The

dumbbell shaped samples have a central part of 35 mm in length, 2 mm in width and around 1 mm in thickness.

Fluorescence spectra were recorded with a Hitachi F-4600 FL Spectrophotometer using Xe lamp as an excitation source. The excitation and emission slits were both set at 5 nm. Fluorescence spectrometry at different temperature was also explored. The temperature control was achieved through a DC-3006 low-temperature thermostat bath, and each temperature was maintained for 2-3 min.

The shape memory properties were quantitatively characterized by a DMA Q800 apparatus under stretching mode with controlled force. The dimension of the Tri-ARA-1-4 strip is 7.45 mm $\times$ 4.14 mm $\times$ 0.60 mm. The Tri-ARA-1-4 was equilibrated at 65 ^{o}C (above T_g) for 10 min. Then an external constant force of 0.045 N was applied, and the temperature was decreased to 10 ^{o}C (below T_g) at a cooling rate of 5 ^{o}C·min^{-1}. After 10 min since the film reached 10 ^{o}C, the external force was reduced to 0.001 N, and the film was reheated to 65 ^{o}C at a heating rate of 5 ^{o}C·min^{-1}. Finally, maintain the temperature at 65 ^{o}C for 10 min. The position changes were recorded in the testing process.

The structure of the synthesized BDATC has a one-to-one correspondence with the peaks of its NMR spectrum. The ^{1}H-NMR spectrum (Fig. S1b) shows characteristic signals of methyl protons at 1.69 ppm. ^{13}C-NMR (DMSO-d_6) (Fig. S1c): δ (ppm) = 219.8, 173.7, 56.8, 25.0. In addition, the structure of BDATC was also characterized by fourier transform infrared spectrum (FT-IR). As shown in Fig. S1d, the bands at 3250-2500 cm^{-1} and the peak at 1700 cm^{-1} can be assigned to the stretching vibration of carboxylic hydroxyl groups and carbonyl, respectively. The absorption peaks at 1450 cm^{-1} 1170 cm^{-1} and 1050 cm^{-1} are corresponded to the vibration of C-C bonds, C=S bonds, and C-O bonds, respectively. Characteristic stretching vibration peaks at 685 cm^{-1} (C-S) also appears.

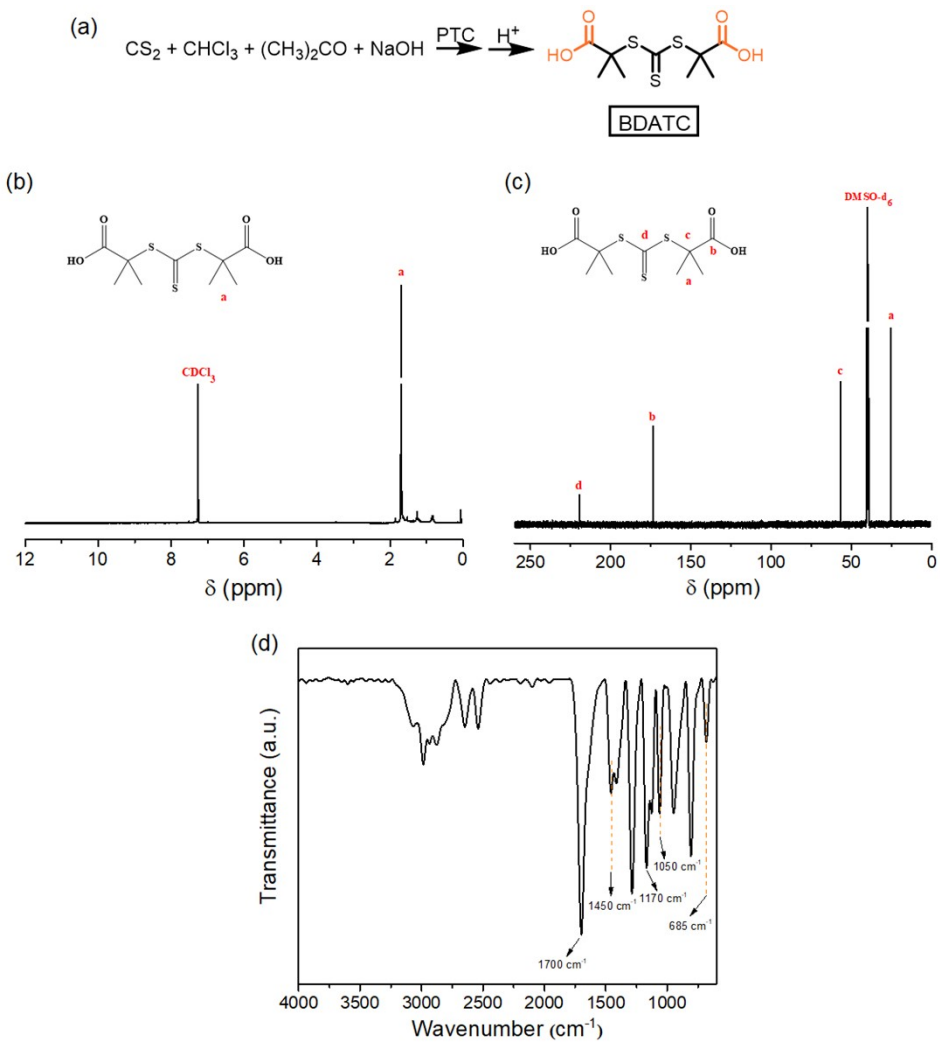

Fig. S1 (a) Synthesis of BDATC. (b) ^{1}H-NMR spectrum, (c) ^{13}C-NMR spectrum and (d) FT-IR spectrum of BDATC.

In order to verify the feasibility of our proposed synthetic strategy, we first studied the polymerization rate of nBA and tBA during copolymerization. NMR spectroscopy was used to detect the monomer conversion during polymerization as well as monomer composition in polymer. Fig. S2 shows the ^{1}H-NMR spectra of P(nBA-co-tBA) samples at distinct time during RAFT polymerization, from which we could Fig. out that the polymerization rates of both nBA and tBA are of tiny difference and have approximate linear relations with the corresponding polymerization time, as shown in Fig. S3. The linear relationship between polymerization rates and time indicates the characteristics of living polymerization. Moreover, combined with the result reported by our group that the reactivity ratios of nBA and tBA during copolymerization are approximately equal and close to 1 [6], we can control the content of carboxyl groups in the

hydrolyzed polymers easily and precisely by adjusting the molar ratio of comonomers. Thus, polymeric materials with different chain structure as well as desired contents of carboxyl groups can be obtained.

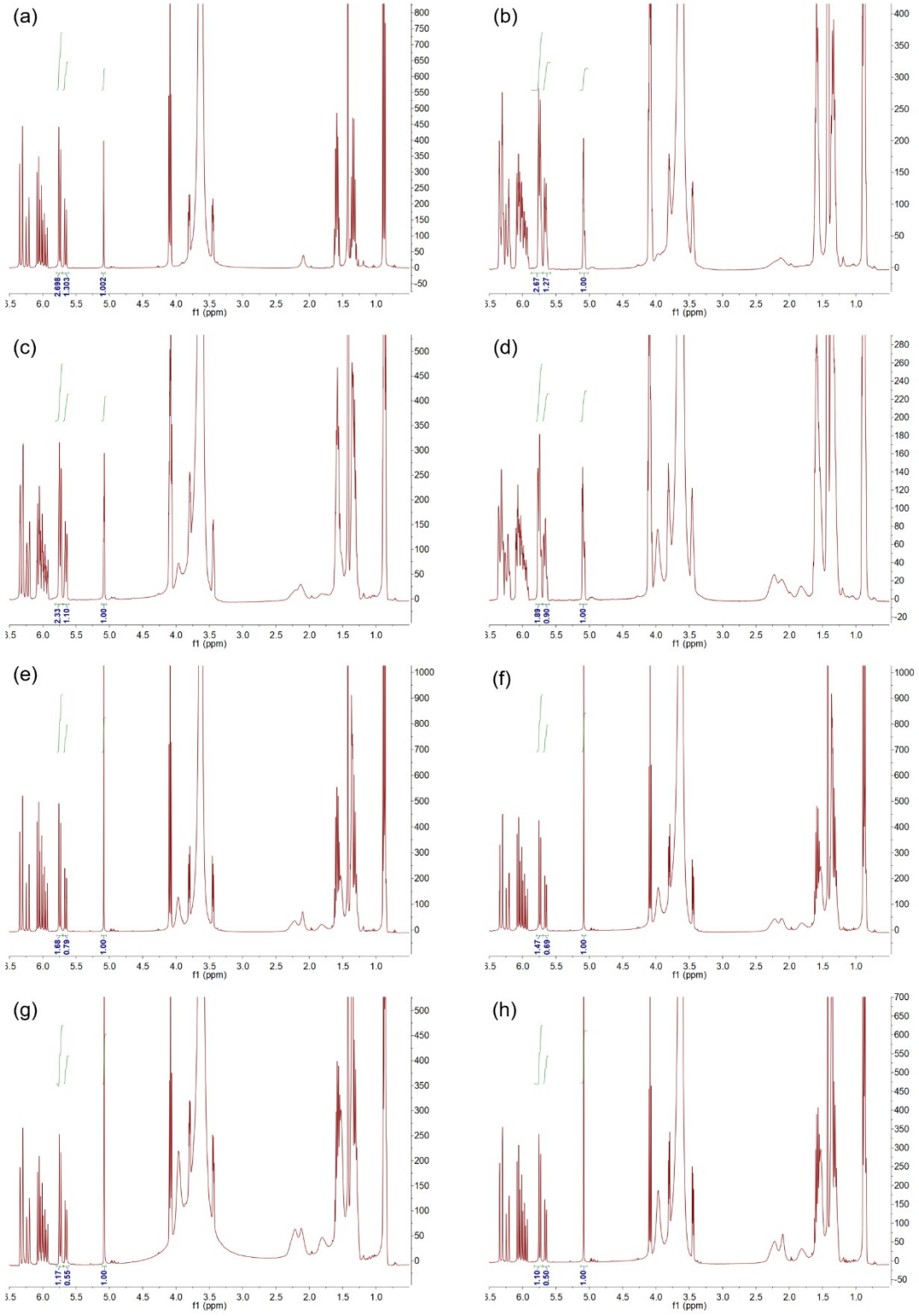

Fig. S2 Time-course ^{1}H-NMR spectra of P(nBA-co-tBA) showing monomer conversion during synthesizing P(nBA-co-tBA) via RAFT polymerization. (a) t = 0 min, (b) t = 14 min, (c) t = 72 min, (d) t = 132 min, (e) t = 176 min, (f) t = 223 min, (g) t = 280 min, (h) t = 311 min.

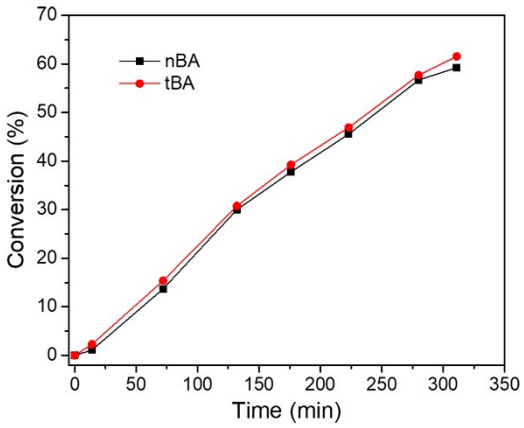

Fig. S3 Conversion-time plots of synthesizing P(nBA-co-tBA) via RAFT polymerization.

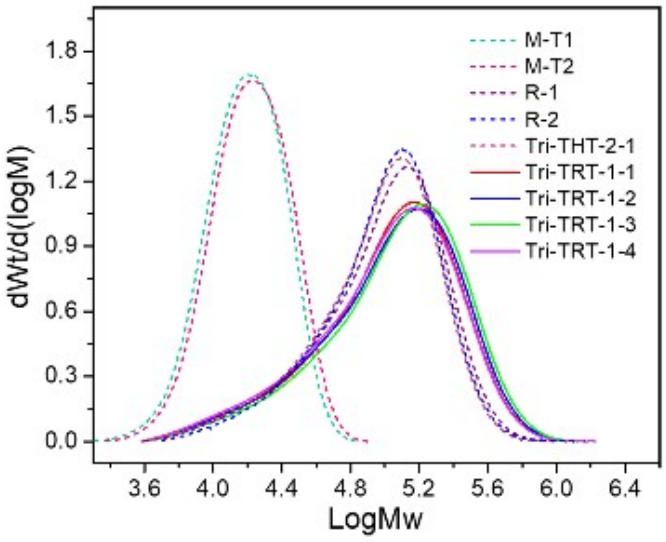

Fig. S4 GPC curves of PtBA macro-RAFT agents and P(nBA-co-tBA) of different chain structures.

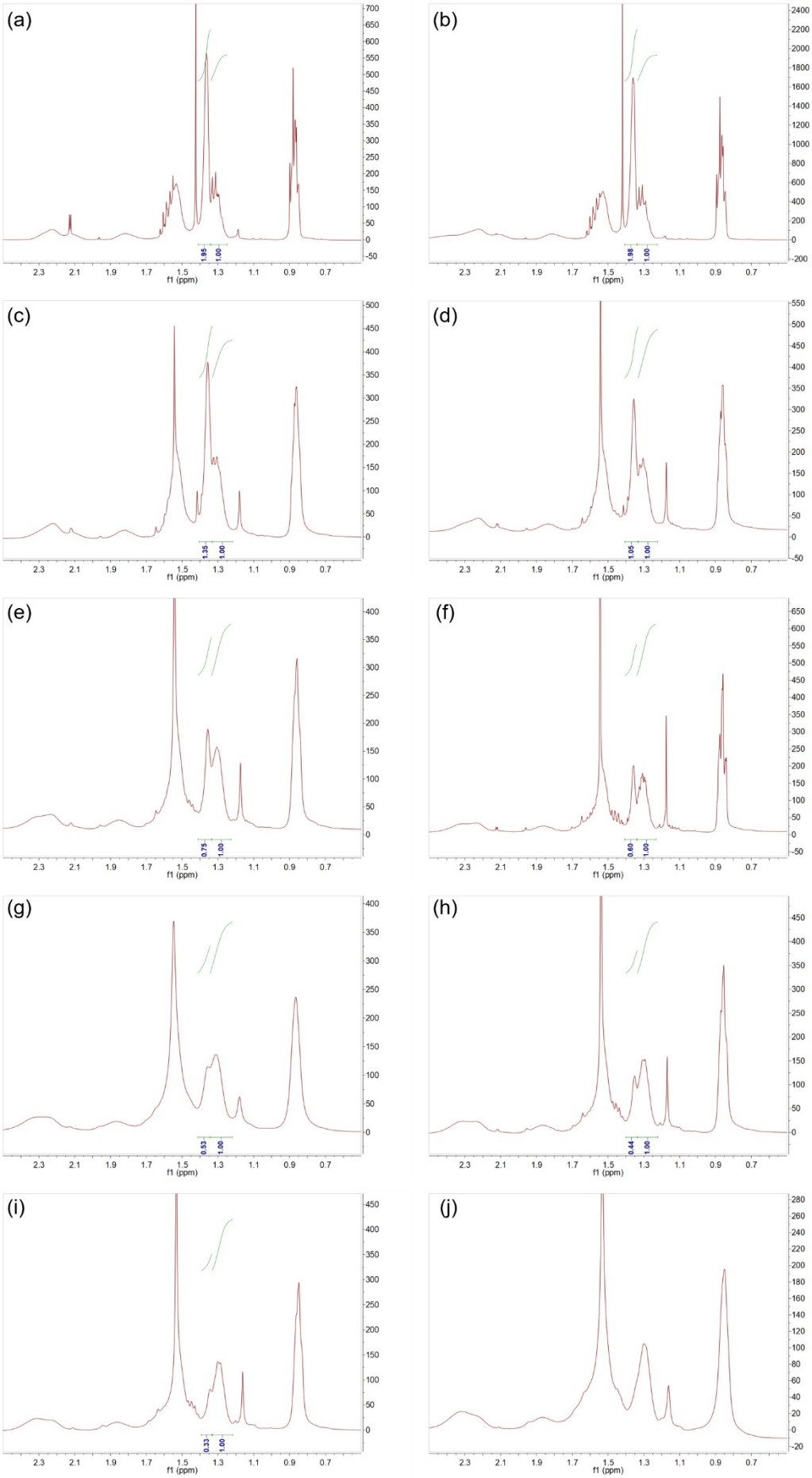
(a)
(b)
(c)
(d)
(e)
(f)
(g)
(h)
(i)
(j)
f1 (ppm)

Fig. S5 The kinetic study of hydrolysis process. (a) 0 h, (b) 0.5 h, (c) 1 h, (d) 2 h, (e) 4.5 h, (f) 5.5 h, (g) 7 h, (h) 8.5 h, (i) 11 h, (j) 14 h.

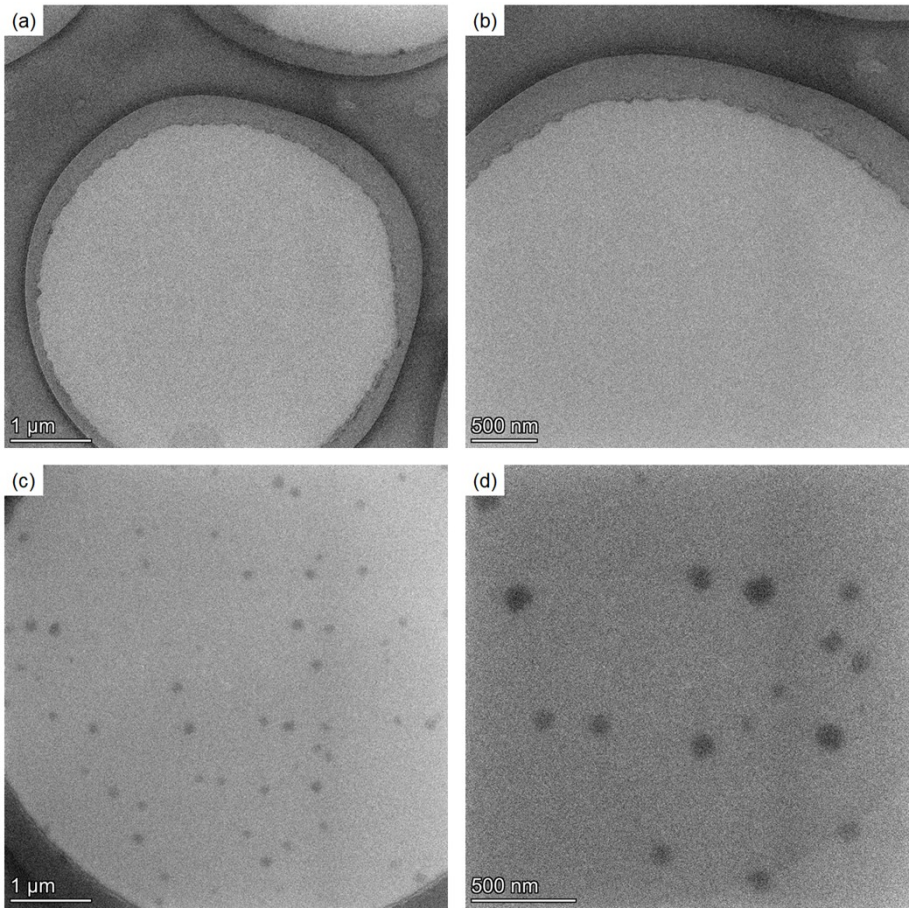

Fig. S6 TEM photograph of Tri-TRT-1-4 (a, b) and Tri-ARA-1-4 (c, d) under different magnification.

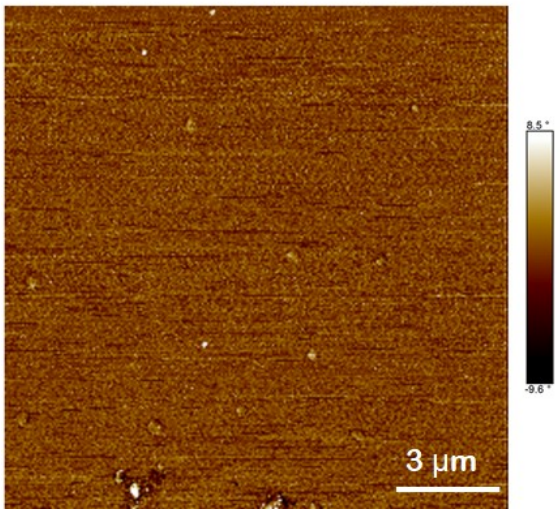

Fig. S7 AFM phase image of Tri-TRT-1-4.

UV-Vis transmission spectrum showed that the Tri-TRT-1-4 film performed excellent transparency in the visible light region since that the transmittance of Tri-TRT-1-4 film with the thickness of 25 µm was around 97% at the wavelength ranging from 400 nm to 800 nm as shown in Fig. S8.

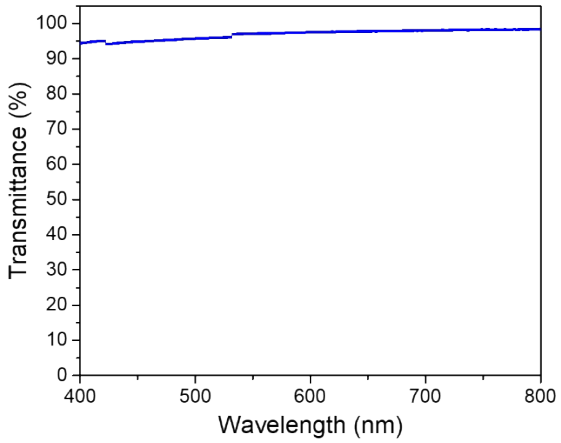

Fig. S8 UV-Vis transmission spectrum of Tri-TRT-1-4 film with the thickness of 25 µm.

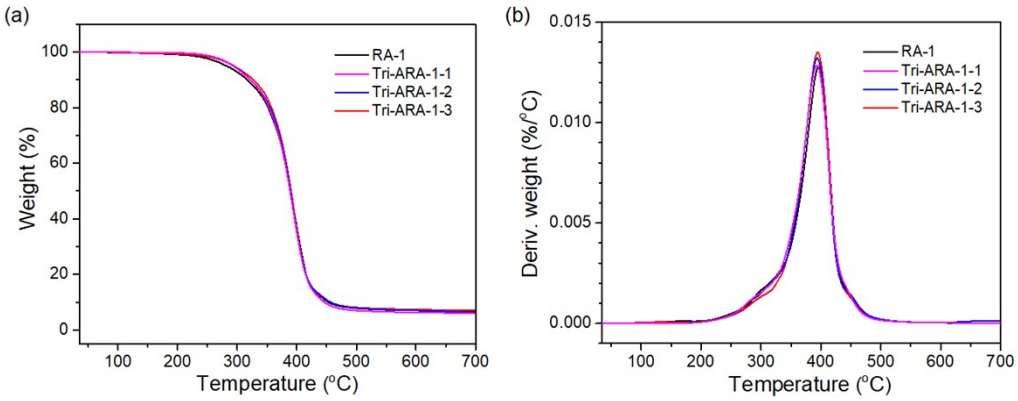

Fig. S9 (a) Thermogravimetric analysis and (b) DTG curves of Tri-ARA-1-4 and reference copolymers including RA-2 and Tri-AHA-2-1.

Taking Tri-TRT-1-4 and Tri-ARA-1-4 for example, the thermal properties before/after hydrolysis were characterized using TGA and DSC. TGA curve of Tri-TRT-1-4 and corresponding derivative thermogravimetry analysis are shown in Fig. S10, from which we can obtain the decomposition temperature of Tri-TRT-1-4 with 5% mass loss (T_{5d}) is about 249.2 °C. And there are two distinct weight loss peaks of pyrolysis around 253.0 °C and 389.9 °C, respectively. The former pyrolytic weight loss peak at 253.0 °C corresponds to the decomposition of tert-butyl groups, while the latter one around 389.9 °C is attributed to the breaking of the macromolecular backbone and the destruction of other chemical bonds. As shown in Fig. 4a and Table S1, T_{5d} of PAA-b-PnBA-b-PAA Tri-ARA-1-4 is 288.2 °C. The conversion of tert-butyl groups to carboxyl groups on the polymer chain increases the thermal stability of the polymer to some extent, but the acidic groups are relatively unstable, so they also break down before the main chain. Besides, from the differential thermal gravity (DTG) curves, Fig. 4b, it can be concluded that there is only one distinct weight loss peak of pyrolysis near 394 °C for Tri-ARA-1-4, which is mainly attributed to the cracking of the macromolecular backbone and the cleavage of chemical bonds. Accordingly, the resultant copolymer after hydrolysis exhibits satisfactory heat resistance.

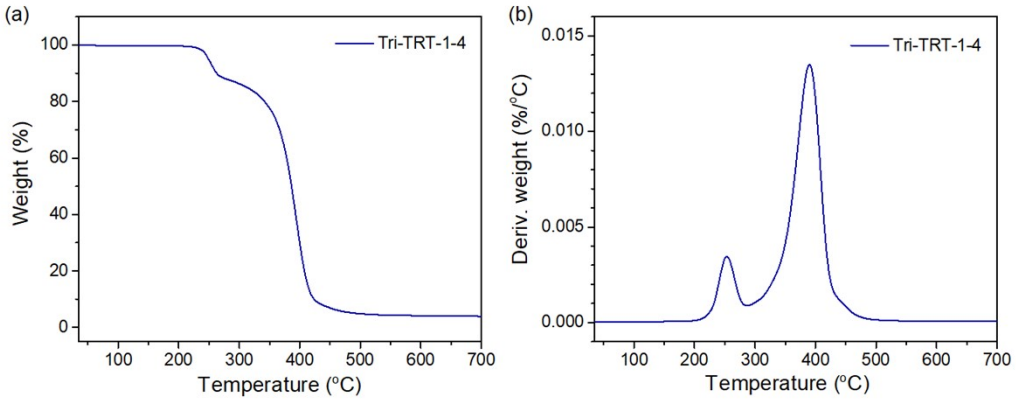

Fig. S10 (a) Thermogravimetric analysis and (b) DTG curves of Tri-TRT-1-4.

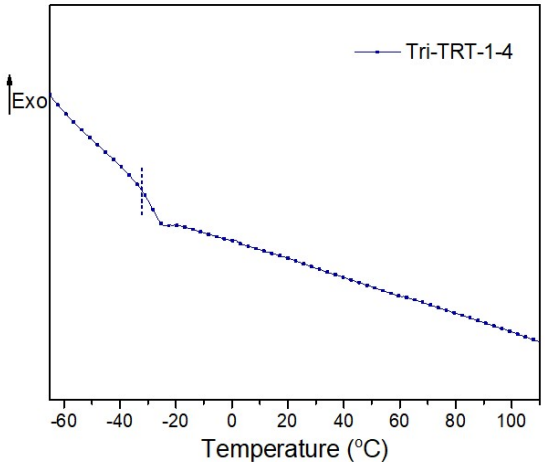

Fig. S11 DSC curve of of Tri-TRT-1-4.

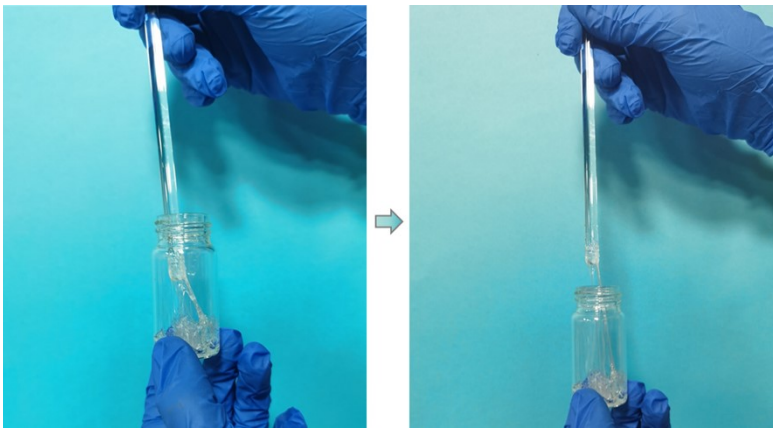

Fig. S12 Check the state of the Tri-TRT-1-4 with a glass rod at room temperature.

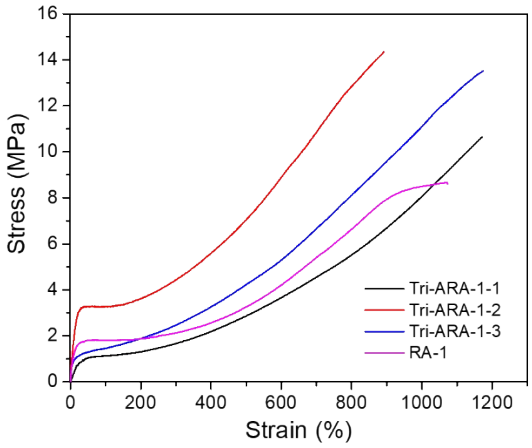

Fig. S13 Stress–strain curves of PAA-b-P(AA-r-nBA)-b-PAA and random copolymer sample.

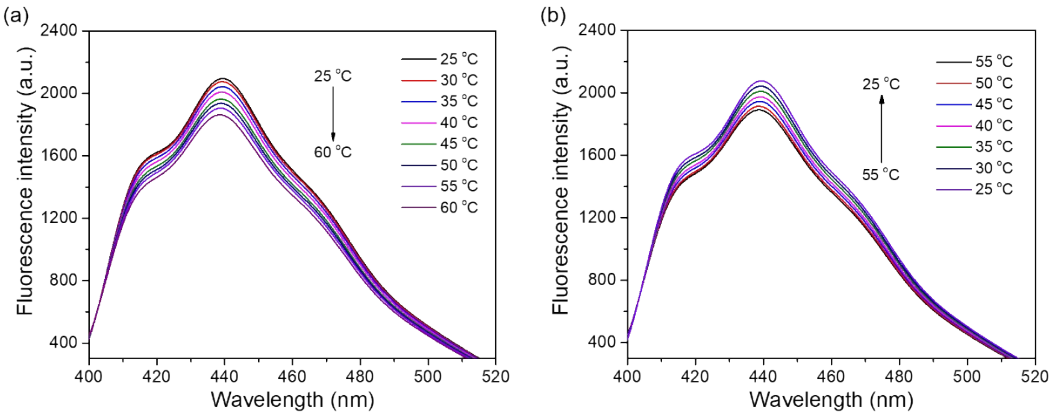

Fig. S14 Fluorescence spectra of 10.43 mg·mL^{-1} of Tri-ARA-1-4 ethanol solution at different temperatures during heating (a) and cooling process (b).

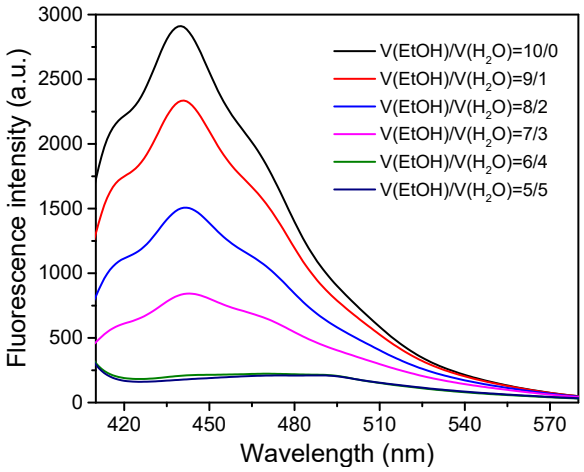

Fig. S15 Curves of the concentration dependence of peak fluorescence emission intensity for Tri-ARA-1-4.

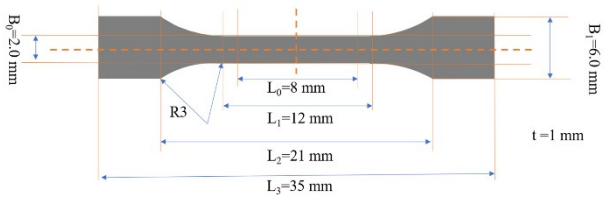

Fig. S16 Shape and detailed size of the test splines.

Insight into the hydrogen bonding interaction of the as-prepared polyacrylates

The high fracture toughness and tensile strength as well as good self-healing performance of the prepared polyacrylates were mainly attributed to the carefully designed distribution of hydrogen bonding. Hence, the property of hydrogen bonding was further investigated. According to the result of our earlier research[6] and other published works[7-8], the existence of hydrogen bonds may cause the movement of polymer molecular chains to be restricted, thus endowing them with the characteristics of fluorescence emission under ultraviolet light. The mechanism is different from that of the traditional chromophore-containing polymers[9-10]. The polyacrylate prepared in this work exhibits strong fluorescence emission under 365 nm UV lamp (Fig. S17a). As an example, the relationship between the concentration of Tri-ARA-1-4 in ethanol and fluorescence intensity was investigated. Results show that the fluorescence emission intensity at 439 nm increases gradually with increasing Tri-ARA-1-4 concentration (Fig. S17b). Tri-ARA-1-4 exhibits an aggregation-

enhanced emission (AEE) effect[11-12] in ethanol solution system. We then investigated temperature responsiveness of the fluorescence intensity of Tri-ARA-1-4. As plotted in Fig. S17d, the fluorescence emission intensity gradually decreases as the temperature increases from 25 °C to 60 °C. Subsequently, the fluorescence emission intensity gradually increases as the temperature drops back down to 25 °C. Such results correspond to the dissociation of the hydrogen bond during the heating process and the re-formation when the temperature is lowered, providing support for the correlation of hydrogen bonding with fluorescence emission and suggesting the existence of hydrogen bonds.

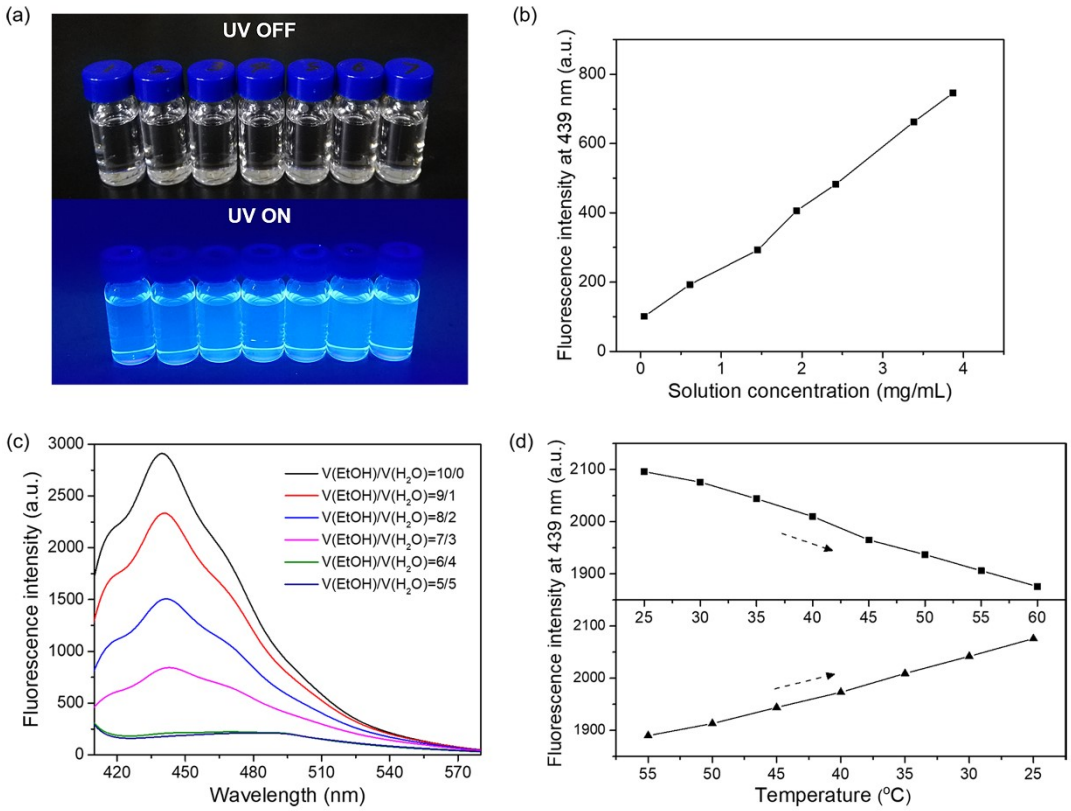

Fig. S17 Photoluminescence properties (a) Photographs of the fluorescence of Tri-ARA-1-4 solutions in daylight (top) and UV light (bottom). (b) Line chart of fluorescence intensity at 439 nm variations over Tri-ARA-1-4 concentration in ethanol. (c) The fluorescence spectra of Tri-ARA-1-4 in mixed solvent comprising ethanol and water at different ratios. (d) Variation of fluorescence emission intensity at 439 nm with temperature during the temperature rise and fall.

Table S1 Formulas used in the synthesis of macro PtBA RAFT agent and copolymers of tBA and nBA.

Sample identification	RAFT agent (mmol)	Monomer tBA (mmol)	Monomer nBA (mmol)	Initiator AIBN (mmol)	Solvent dioxane(mL)	nBA/tBA ratio [d]
M-T1	0.3752 [a]	55.11	-	0.1876	25	-
M-T2	0.3752 [a]	68.89	-	0.2113	30	-
Tri-TRT-1-1	0.04271 [b]	23.56	101.6	0.02314	35	3.77/1
Tri-TRT-1-2	0.04261 [b]	24.58	100.3	0.02314	35	3.35/1
Tri-TRT-1-3	0.04259 [b]	25.83	99.32	0.02314	35	3.22/1
Tri-TRT-1-4	0.04270 [b]	26.61	98.54	0.02375	35	3.06/1
R-1	0.02199 [a]	14.82	51.18	0.01157	18	3.23/1
R-2	0.02234 [a]	15.21	50.32	0.01157	18	3.12/1
Tri-THT-2-1	0.02116 [c]	-	63.12	0.01279	18	3.00/1

a) S, S'-Bis (α, α'-dimethyl-α''-acetic acid) trithiocarbonate (BDATC) used as chain transfer agent; b) Macro PtBA 1 (M_n = 11350) employed as chain transfer agent; c) Macro PtBA 2 (M_n = 14379) employed as chain transfer agent; d) nBA/tBA ratio Fig.d out employing ^{1}H-NMR spectrum.

Table S2 Thermal performance index of the investigated hydrolyzed copolymer.

Sample		T_{5d} (°C)
PAA_m-b-P(AA-r-nBA)-b-PAA_m	Tri-ARA-1-1	292.9
	Tri-ARA-1-2	293.7
	Tri-ARA-1-3	294.5
	Tri-ARA-1-4	288.2
P(AA-r-nBA)	RA-1	282.2
	RA-2	287.0
PAA_n-b-PnBA-b-PAA_n	Tri-AHA-2-1	327.7

Table S3 Tensile mechanical property of the acid-hydrolysis products of PtBA-b-P(tBA-r-nBA)-b-PtBA and the control samples.

Sample identification	nBA/AA ratio	Tensile strength (MPa)	Fracture strain (%)	Fracture toughness (MJ/m^3)

Tri-ARA-1-1	3.77/1	11.14 ± 0.64	1209 ± 85	54.94 ± 2.35
Tri-ARA-1-2	3.35/1	14.35 ± 0.10	891 ± 32	64.08 ± 2.71
Tri-ARA-1-3	3.22/1	13.52 ± 0.77	1175 ± 28	68.44 ± 8.65
Tri-ARA-1-4	3.06/1	20.96 ± 1.88	596 ± 4	77.06 ± 7.98
RA-1	3.23/1	8.52 ± 0.20	1094 ± 33	46.25 ± 1.01
RA-2	3.12/1	16.16 ± 1.16	622 ± 12	66.55 ± 3.76
Tri-AHA-2-1	3.00/1	0.47 ± 0.06	849 ± 83	2.22 ± 0.23

Table S4 The comparison of the mechanical strength of Tri-ARA samples and other noncovalent cross-linked polymers with microphase-separated structure and self-healing ability reported in the literatures.

The mark in Fig. 7c	Sample name	Tensile strength (MPa)	Fracture strain (%)	Healing conditions	Ref.
1	P-Cur-Eu = 3:1	1.8	900	48 h at 25 °C	42
2	PUDS-6	18	1800	12 h at 70 °C	43
3	PU1/5-AHMP-0.75	5.51	873	in air for24 h	44
4	PU1/5-AHMP-1.0	23.89	4	in air for24 h	44
5	HBP-3	3.77	310	at room temperature for 24 h	23
6	HBP-2	1.92	780	at room temperature for 24 h	23
7	BCP1	4.38	732	at room temperature 10for 24 h	45
8	BCP2	6.07	316	at room temperature for 24 h	45
9	PDMS-MPI	1.45	954	at room temperature for 4 h	46
10	elastomer 3	12.20	354	over 37 °C	47
11	elastomer 2	4.48	2231	at 37 °C for 24 h	47
12	(PA-amide)-88@PS	2.0	18	at room temperature for 24 h	48
13	ICP-2 L/Zn = 4.0	1.45	760	under ambient	49

				conditions for 3 h	
14	P2/Zn-a	3.45	490	at 40 °C for 24 h	50
15	DP 500, 20%	2.87	1214	at ambient temperature for 24 h	51
16	Poly-2	1.35	600	45 °C for 18 h	52
17	PISi-1500-4	2.07	75	at room temperature for 16 h	53
18	PU20-b-P(D320-r-U40)-b-PU20	16.3	716	at 50 °C for 3 h	54
19	Poly-CD 1.5 mol%	6.78	950	under ambient conditions	55
20	Iron-MN	14	480	at room temperature for 6 h	56
Tri-ARA-1-1	Tri-ARA-1-1	11.14	1209	at room temperature for 24 h	This work
Tri-ARA-1-2	Tri-ARA-1-2	14.35	891	at room temperature for 24 h	This work
Tri-ARA-1-3	Tri-ARA-1-3	13.52	1175	at room temperature for 24 h	This work
Tri-ARA-1-4	Tri-ARA-1-4	20.96	596	at room temperature for 24 h	This work

References

(1) Wei, K.; Wang, L.; Li, L.; Zheng, S. Synthesis and Characterization of Bead-Like Poly (N-Isopropylacrylamide) Copolymers with Double Decker Silsesquioxane in the Main Chains. *Polym. Chem.* **2015,** *6*, 256-269.

(2) Lai, J. T.; Filla, D.; Shea, R. Functional Polymers from Novel Carboxyl-Terminated Trithiocarbonates as Highly Efficient Raft Agents. *Macromolecules* **2002,** *35*, 6754-6756.

(3) Bouchékif, H.; Narain, R. Reversible Addition− Fragmentation Chain Transfer Polymerization of N-Isopropylacrylamide: A Comparison between a Conventional and a Fast Initiator. *J. Phys. Chem. B* **2007,** *111*, 11120-11126.

(4) Nuopponen, M.; Kalliomäki, K.; Laukkanen, A.; Hietala, S.; Tenhu, H. A–B–a Stereoblock Copolymers of N-Isopropylacrylamide. *J. Polym. Sci. Pol. Chem.* **2008,** *46*, 38-46.

(5) Kirkland, S. E.; Hensarling, R. M.; McConaughy, S. D.; Guo, Y.; Jarrett, W. L.; McCormick, C. L. Thermoreversible Hydrogels from Raft-Synthesized Bab Triblock Copolymers: Steps toward Biomimetic Matrices for Tissue Regeneration. *Biomacromolecules* **2008,** *9*, 481-486.

(6) Wang, W.; Liu, Z.; Guo, Z.; Zhang, J.; Li, C.; Qiu, S.; Lei, X.; Zhang, Q. Hydrogen Bonding-Derived Healable Polyacrylate Elastomers Via on-Demand Copolymerization of N-Butyl Acrylate and Tert-Butyl Acrylate. *ACS Appl. Mater. Inter.* **2020,** *12*, 50812-50822.

(7) Song, L. Z.; Zhu, T. Y.; Yuan, L.; Zhou, J. J.; Zhang, Y. Q.; Wang, Z. K.; Tang, C. B. Ultra-Strong Long-Chain Polyamide Elastomers with Programmable Supramolecular Interactions and Oriented Crystalline Microstructures. *Nat. Commun.* **2019,** *10*, 1-8.

(8) Chen, X. X.; Zhong, Q. Y.; Cui, C. H.; Ma, L.; Liu, S.; Zhang, Q.; Wu, Y. S.; An, L.; Cheng, Y. L.; Ye, S. B.; Chen, X. M.; Dong, Z.; Chen, Q.; Zhang, Y. F. Extremely Tough, Puncture-Resistant, Transparent, and Photoluminescent Polyurethane Elastomers for Crack Self-Diagnose and Healing Tracking. *ACS Appl. Mater. Inter.* **2020,** *12*, 30847-30855.

(9) Friend, R.; Gymer, R.; Holmes, A.; Burroughes, J.; Marks, R.; Taliani, C.; Bradley, D.; Dos Santos, D.; Bredas, J.; Lögdlund, M. Electroluminescence in Conjugated Polymers. *Nature* **1999,** *397*, 121-128.

(10) Toal, S. J.; Jones, K. A.; Magde, D.; Trogler, W. C. Luminescent Silole Nanoparticles as Chemoselective Sensors for Cr (Vi). *J. Am. Chem. Soc.* **2005,** *127*, 11661-11665.

(11) Niu, S.; Yan, H.; Chen, Z.; Yuan, L.; Liu, T.; Liu, C. Water-Soluble Blue Fluorescence-Emitting Hyperbranched Polysiloxanes Simultaneously Containing Hydroxyl and Primary Amine Groups. *Macromol. Rapid Comm.* **2016,** *37*, 136-142.

(12) Liu, J.; Zhong, Y.; Lu, P.; Hong, Y.; Lam, J. W.; Faisal, M.; Yu, Y.; Wong, K. S.; Tang, B. Z. A Superamplification Effect in the Detection of Explosives by a Fluorescent Hyperbranched Poly (Silylenephenylene) with Aggregation-Enhanced Emission Characteristics. *Polym. Chem.* **2010,** *1*, 426-429.